Trimer-based spin liquid candidate $Ba_4NbIr_3O_{12}$

Loi T. Nguyen and R. J. Cava
Department of Chemistry, Princeton University, Princeton, New Jersey 08544, USA

(Received 4 November 2018; published 23 January 2019)

$Ba_4NbIr_3O_{12}$, a material with a triangular planar geometry of Ir_3O_{12} trimers, is described. Magnetic susceptibility measurements show it to be paramagnetic with no magnetic ordering down to 1.8 K despite the Curie-Weiss temperature (θ_{CW}) of −13 K. The material has a very low effective magnetic moment (μ_{eff}) of 0.80 μ_B/f.u. To look at the lower-temperature behavior, the specific heat (C_p) was measured down to 0.35 K; it shows no indication of magnetic ordering and fitting a power law to C_p vs T below 2 K yields the power $\alpha = 3/4$. Comparison to the trimer compound made with the 4*d* element Rh in place of the 5*d* element Ir, $Ba_4NbRh_3O_{12}$, which is also paramagnetic ($\mu_{eff} = 1.48\mu_B$/f.u., $\theta_{CW} = -23$ K), is presented. The analysis suggests that $Ba_4NbIr_3O_{12}$ is a candidate spin liquid material.

DOI: 10.1103/PhysRevMaterials.3.014412

I. INTRODUCTION

Spin-orbit coupling (SOC), the interaction between the spin of an electron and the magnetic field present in its orbit around a heavy nucleus, has proven to be an important factor for understanding the magnetic properties and insulating state in many iridium-based oxides [1–5]. In an octahedral crystal field, in the absence of SOC, the *d* orbitals split into triply degenerate t_{2g} and doubly degenerate e_g states, but SOC can further split the t_{2g} manifold into two discrete energy levels, i.e., a quartet $J = 3/2$ and doublet $J = 1/2$. The importance of SOC for understanding the magnetism in Ir-based compounds therefore depends on the number of electrons in the 5*d* manifold of electronic states. Here we consider a system with two formally Ir^{4+} ($5d^5$) and one formally Ir^{3+} ($5d^6$) present. Spin liquid behavior, the spin Hall effect [6], the topological Weyl semimetallic state, and Mott insulator states [3,7,8] are all present in iridates, which have also been of recent interest because spin liquid states may be stable at low temperatures in some of these materials [9–11]. $Na_4Ir_3O_8$, for example, a garnet-related oxide, displays large magnetic specific heat at low temperature and was reported to have a spin liquid ground state [10]. Also, recently, a quantum spin liquid state in $H_3LiIr_2O_6$ has been published [11]. Thus new iridate materials with exotic magnetic properties are of significant interest.

Here we describe an Ir-trimer-based compound, $Ba_4NbIr_3O_{12}$, which displays a rhombohedral structure with the space group *R*-3*m* (No. 166). The rhombohedral symmetry displayed is in contrast to the monoclinic symmetry (*C*2/*m*) found for materials in the related $Ba_4LnIr_3O_{12}$ (Ln = lanthanide) family. The presence of Ir trimers in this material, made from three face-sharing IrO_6 octahedra, is significant because whether the material acts as a "molecular" or "point charge" magnetic system is a question of interest [12]. In addition, we describe $Ba_4NbRh_3O_{12}$, which forms Rh_3O_{12} trimers. The comparison is of interest due to the fact that the materials are based on magnetically active 5*d* (Ir) and 4*d* (Rh) elements with the same number of valence electrons. Neither compound shows any magnetic ordering down to 1.8 K even though the absolute values of their Curie-Weiss temperatures are larger than 1.8 K,−13.1 K for $Ba_4NbIr_3O_{12}$, and −23.2 K for $Ba_4NbRh_3O_{12}$. Magnetic measurements reveal an effective moment of $0.80\mu_B$/f.u. for $Ba_4NbIr_3O_{12}$ and $1.48\mu_B$/f.u. for $Ba_4NbRh_3O_{12}$. Resistivity measurements show that both compounds are semiconductors with transport gaps of about 0.05 eV. $Ba_4NbRh_3O_{12}$ shows a feature in its specific heat that can be interpreted as being the result of magnetic ordering at 1.5 K. $Ba_4NbIr_3O_{12}$, on the other hand, displays a linear upturn in C_p/T at low temperatures and appears to be a candidate for a spin liquid.

II. EXPERIMENT

Polycrystalline samples of $Ba_4NbIr_3O_{12}$ and $Ba_4NbRh_3O_{12}$ were synthesized by solid-state reaction using $BaCO_3$, Nb_2O_5, IrO_2, and RhO_2 (Alfa Aesar, 99.9%, 99.5%, 99.9%, and 99.9%, respectively) in stoichiometric ratios as starting materials. Reagents were mixed thoroughly, placed in alumina crucibles, and heated in air at 900 °C for 24 hours. The resulting powders were reground, pressed into pellets, and heated in air at 1100 °C for 48 hours. The phase purities and crystal structures were determined through powder x-ray diffraction (PXRD) using a Bruker D8 Advance Eco with Cu Kα radiation and a LynxEye-XE detector. The structural refinements were performed with GSAS [13]. The crystal structure drawings were created by using the program VESTA [14].

The magnetic susceptibilities of $Ba_4Nb\mathit{M}_3O_{12}$ (M= Ir or Rh) powders were measured in a Quantum Design Physical Property Measurement System (PPMS) DynaCool equipped with a VSM option. The magnetic susceptibilities between 1.8 and 300 K, defined as M/H, where M is the sample magnetization and H is the applied field, were measured at the field of H= 5 kOe for $Ba_4NbIr_3O_{12}$ and 2 kOe for $Ba_4NbRh_3O_{12}$; some additional measurements were performed in an applied field of 100 Oe. The resistivities were

TABLE I. Structural parameters for $Ba_4NbIr_3O_{12}$ and $Ba_4NbRh_3O_{12}$ at 300 K. Both compounds crystallize in the *R*-3*m* space group (No. 166) in International Tables for Crystallography.

Atom	Wyckoff.	Occ.	*x*	*y*	*z*	U_{iso}
			$Ba_4NbIr_3O_{12}$			
Ba1	6*c*	1	0	0	0.12890(6)	0.0302(7)
Ba2	6*c*	1	0	0	0.28585(7)	0.0326(8)
Nb	3*a*	1	0	0	0	0.0008(4)
Ir1	3*b*	1	0	0	½	0.0298(4)
Ir2	6*c*	1	0	0	0.41148(6)	0.0386(7)
O1	18*h*	1	0.4817(7)	0.5183(7)	0.1216(3)	0.067(5)
O2	18*h*	1	0.5146(6)	0.4854(6)	0.2956(4)	0.066(4)
$a = 5.7827(2)$Å, $c = 28.7725(9)$Å						
$\chi^2 = 1.38$, $R_{wp} = 5.79\%$, $R_p = 4.48\%$, $R_F^2 = 6.09\%$						
			$Ba_4NbRh_3O_{12}$			
Ba1	6*c*	1	0	0	0.12843(9)	0.0229(9)
Ba2	6*c*	1	0	0	0.28570(9)	0.0224(9)
Nb	3*a*	1	0	0	0	0.0090(3)
Rh1	3*b*	1	0	0	½	0.0115(8)
Rh2	6*c*	1	0	0	0.4106(1)	0.0115(8)
O1	18*h*	1	0.4848(4)	0.5152(8)	0.1202(4)	0.002(4)
O2	18*h*	1	0.510(1)	0.490(1)	0.2911(7)	0.077(6)
$a = 5.75707(4)$Å, $c = 28.4734(5)$Å						
$\chi^2 = 2.47$, $R_{wp} = 5.89\%$, $R_p = 4.44\%$, $R_F^2 = 9.57\%$						

measured by the dc four-contact method in the temperature range 200 to 300 K in the PPMS. For the resistivity measurements, the samples were pressed, sintered, and cut into pieces with the approximate size $1.0 \times 2.0 \times 1.0\,mm^3$. Four Pt contact wires were connected to the samples using silver paint. The specific heat was measured from 10 to 1.8 K by a PPMS DynaCool equipped with a heat-capacity option, and by using a ^{3}He system to reach down to 0.35 K.

III. RESULTS AND DISCUSSION

The powder x-ray diffraction patterns and structural refinements for $Ba_4NbIr_3O_{12}$ and $Ba_4NbRh_3O_{12}$ are shown in Figs. 1. and 2. The structure of $Ba_4NbRu_3O_{12}$ [12] was used as the starting model for the structure refinements. The agreement between the observed and calculated patterns is excellent. There is no long-range charge ordering within the trimer evident in the structural characterization that we performed.

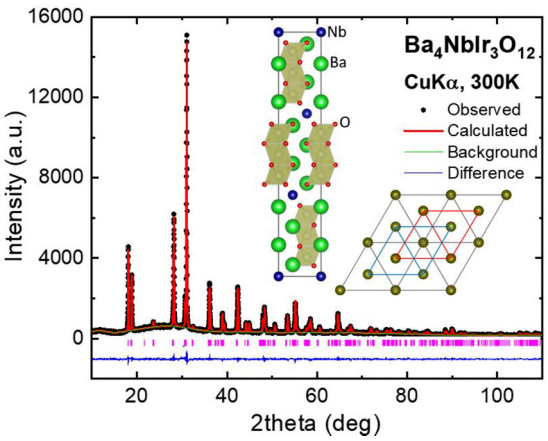

FIG. 1. Rietveld powder x-ray diffraction refinement for $Ba_4NbIr_3O_{12}$ in space group *R*-3*m*. The observed x-ray pattern is shown in black, calculated in red, difference (I_{obs}-I_{calc}) in blue, and the tick marks denote the allowed peak positions in pink. $R_p = 0.0448$, $R_{wp} = 0.0579$, $\chi^2 = 1.38$. The left inset shows the trimer crystal structure (Ir_3O_{12} trimers are shaded yellow) and the right inset shows that the trimers are arranged in an ABC packing array.

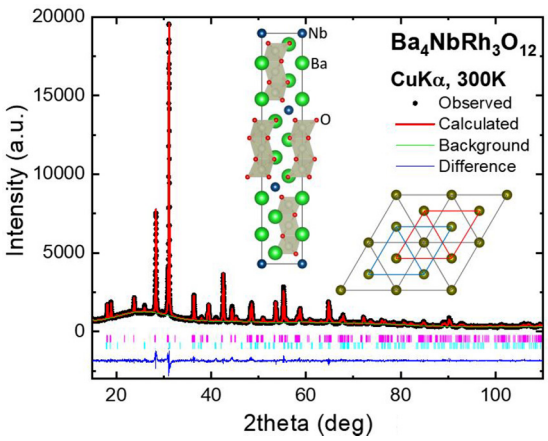

FIG. 2. Rietveld powder x-ray diffraction refinement for $Ba_4NbRh_3O_{12}$ in space group *R*-3*m*. The observed x-ray pattern is shown in black, calculated in red, difference (I_{obs}-I_{calc}) in blue, and the tick marks denote the allowed peak positions in pink ($Ba_4NbRh_3O_{12}$) and in cyan ($BaRhO_3$). $R_p = 0.0439$, $R_{wp} = 0.0578$, $\chi^2 = 2.47$. The left inset shows the trimer crystal structure (Rh_3O_{12} trimers are shaded gray) and the right inset shows that the trimers are arranged in an ABC packing array.

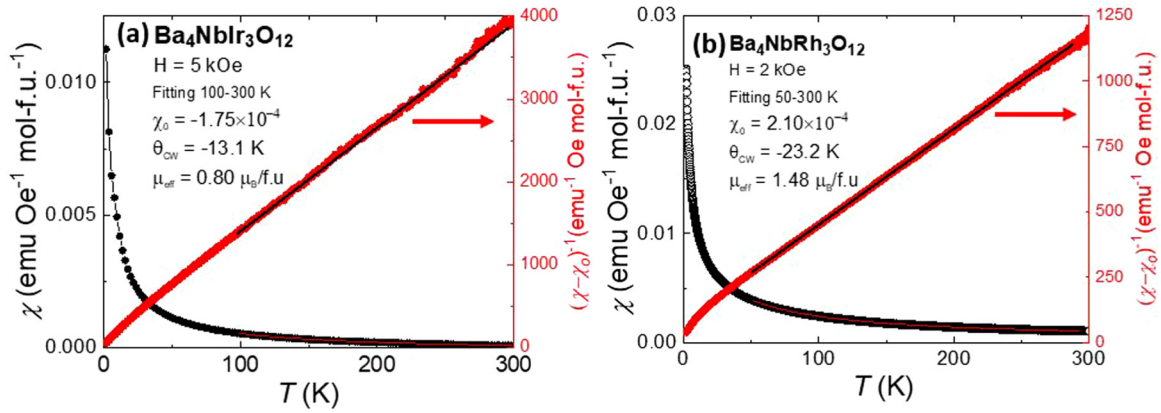

FIG. 3. The temperature dependence of the magnetic susceptibility and the inverse of the difference between the magnetic susceptibility and the temperature-independent magnetic susceptibility (χ_0) for (a) $Ba_4NbIr_3O_{12}$ and (b) $Ba_4NbRh_3O_{12}$. The red solid lines are the fits to the Curie-Weiss law.

Both $Ba_4NbIr_3O_{12}$ and $Ba_4NbRh_3O_{12}$ are rhombohedral, with the space group R-3m (No. 166). The lattice parameters and structural parameters for both compounds are summarized in Table I. Their structure consists of three MO_6 (M= Ir or Rh) octahedra connected by face sharing to form M_3O_{12} trimers. The trimers are arranged in a triangular planar lattice. While $Ba_4LnIr_3O_{12}$ (Ln = lanthanides) have the monoclinic $C2/m$ space group, $Ba_4NbIr_3O_{12}$ adopts a higher-symmetry R-3m crystal structure [15,16]. The individual NbO_6 octahedra and M_3O_{12} trimers in these $Ba_4NbM_3O_{12}$ phases alternate along c to generate the 12-layer (i.e., three layers of four octahedra) hexagonal perovskite structure. Individual M_3O_{12} trimers are corner sharing with the nonmagnetic NbO_6 octahedra, and not to other trimers, such that the magnetic coupling between trimers is of the M-O-O-M super-super exchange type. Structure refinements in which the Ir or Rh to Nb ratio was allowed to vary were highly unsatisfactory, thus confirming the composition of the materials. To the resolution of the structural determination, the Nb:Ir and Nb:Rh sublattices are fully ordered.

The temperature-dependent magnetic susceptibility of $Ba_4NbIr_3O_{12}$ and its reciprocal are plotted in Fig. 3(a). The data from 100 to 300 K are well fit to the Curie-Weiss law $\chi = \frac{C}{T-\theta_{CW}} + \chi_o$, where χ_o is the temperature-independent part of the susceptibility, C is the Curie constant, and θ_{CW} is the Curie-Weiss temperature. The least-squares fitting yields $\chi_o = -1.75 \times 10^{-4}$emu Oe^{-1}mol-f.u.$^{-1}$, $\mu_{eff} = 0.80\mu_B$/f.u., and $\theta_{CW} = -13.1$ K. The measured susceptibilities are consistent among the different samples of each material measured and consistent with the specific-heat measurements. If one insists, however, that the bulk materials must be nonmagnetic and that the observed magnetic susceptibilities must arise from magnetic impurities, then that would require 8% of a spin-1 impurity for $Ba_4NbIr_3O_{12}$ and 27% of a spin-1 impurity for the Rh material, which are orders of magnitude larger than what is possible for our syntheses. Similar magnetic behavior was observed in $Ba_5AlIr_2O_{11}$ [17], which has a Curie-Weiss temperature of -14 K and effective moment of $1.04\mu_B$/f.u. The effective moment of $Ba_4NbIr_3O_{12}$ is smaller than the one observed in $Ba_4Ni_{1.94}Ir_{2.06}O_{12}$, which has a mixed trimer between Ir and Ni [18]. Similar characterization of $Ba_4NbRh_3O_{12}$ gives $\chi_o = 2.10 \times 10^{-4}$emu Oe^{-1}mol-f.u.$^{-1}$, $\mu_{eff} = 1.48\mu_B$/f.u., and $\theta_{CW} = -23.2$ K, as illustrated in Fig. 3(b). Ir and Rh are in the same

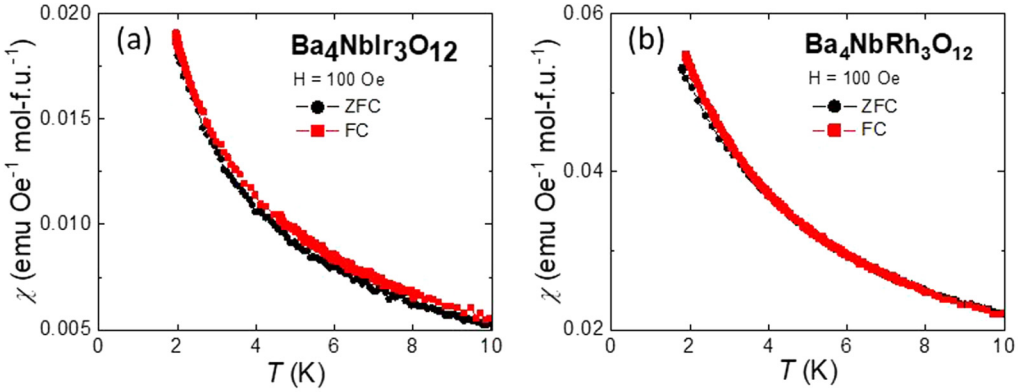

FIG. 4. Field-cooled (FC) and zero-field-cooled (ZFC) dc magnetic susceptibility in an applied field of 100 Oe for (a) $Ba_4NbIr_3O_{12}$ and (b) $Ba_4NbRh_3O_{12}$ from 1.8 to 10 K. There is no bifurcation between FC and ZFC dc magnetic susceptibility down to 1.8 K in the former material and a small amount below 2 K in the latter.

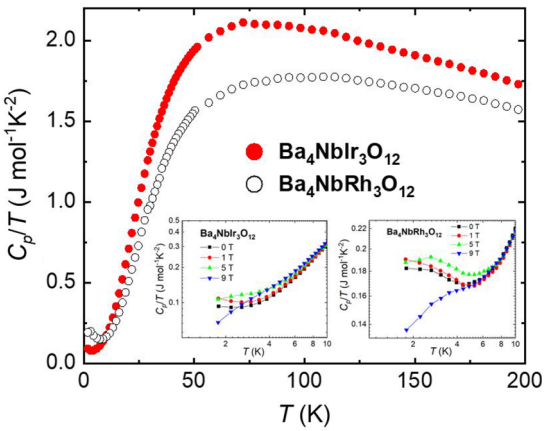

FIG. 5. Molar heat capacity divided by temperature for $Ba_4NbIr_3O_{12}$ (red circles) and $Ba_4NbRh_3O_{12}$ (black open circles) measured from 1.8 to 200 K. Inset: Both materials show features below 10 K. The upturn in C_p/T is suppressed by magnetic field (5 and 9 T) in the Ir case. However, it is the tail of the lower-temperature hump in the Rh case.

column of the periodic table, with Rh being a 4*d* element and Ir being a 5*d* element; the differences in effective moments in the materials may come from the mixed valency of the Ir and Rh combined with metal-oxygen covalency. The relatively low overall moments are of interest as characteristics that should be explained in any theoretical treatment of these materials. The temperature-dependent magnetic susceptibilities of $Ba_4NbIr_3O_{12}$ and $Ba_4NbRh_3O_{12}$ under different applied fields are shown in the Supplemental Material, Figs. S1 [27].

Different from the case of $Ba_4Ni_{1.94}Ir_{2.06}O_{12}$ [16] where the magnetization comes from both the Ir_2NiO_{12} trimers and the isolated $Ni^{2+}O_6$ octahedra, in $Ba_4NbM_3O_{12}$, where both Ba^{2+} and Nb^{5+} are nonmagnetic, the magnetic properties of the $Ba_4NbM_3O_{12}$ materials studied here are determined by the intertrimer and intratrimer interactions of the M_3O_{12} "molecular" units; we postulate, although theoretical treatment is outside the scope of this study and would be of interest, that the system is best considered as each trimer acting as an electronic and magnetic building block in this material, with *M*2-*M*1-*M*2 bonding interactions within the trimers. The resulting antiferromagnetic interactions lead to $\theta_{CW} = -13.1$ K for the Ir case and -23.2 K for the Rh case.

Figures 4(a) and 4(b) show the field-cooled (FC) and zero-field-cooled (ZFC) dc susceptibility in an applied field of 100 Oe for $Ba_4NbIr_3O_{12}$ and $Ba_4NbRh_3O_{12}$. In both compounds, the magnetic susceptibility increases down to the lowest measured temperature of 1.8 K. Combined with relatively large negative Curie-Weiss temperature, the behavior in the ZFC/FC dc susceptibility indicates the possibility of magnetic frustration (frustration index $= |\theta_{CW}|/T_M \approx 7$ for the Ir case and 12 for the Rh case) or even spin liquid behavior in these materials.

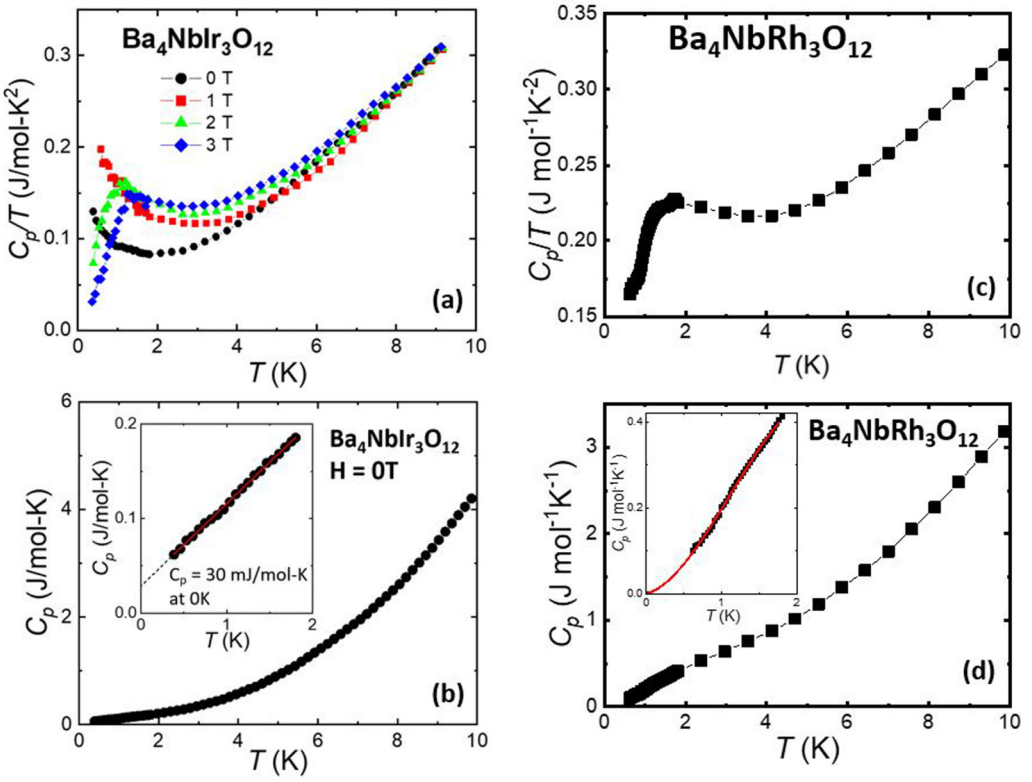

FIG. 6. (a),(c) Low-temperature molar heat capacity divided by temperature for $Ba_4NbIr_3O_{12}$ and $Ba_4NbRh_3O_{12}$. The linear upturn (red line) at the lowest temperature suggests that $Ba_4NbIr_3O_{12}$ is a candidate spin liquid (also see Fig. S3 of the Supplemental Material [27]), while the broad hump in the C_p/T vs T plot of $Ba_4NbRh_3O_{12}$ could reflect the formation of a glassy state. (b),(d) Molar heat capacity of $Ba_4NbIr_3O_{12}$ and $Ba_4NbRh_3O_{12}$, respectively, from 10 to 0.35 K.

Figure 5 shows the specific heat divided by temperature for $Ba_4NbIr_3O_{12}$ and $Ba_4NbRh_3O_{12}$ in the temperature range from 1.8 to 200 K. There is no anomaly, indicating the absence of long-range magnetic order or phase transitions in this temperature range. We note that at 200 K, C_p has not yet reached the saturation value of $3NR$ (N is the number of atoms in one formula unit), but this observed behavior is often encountered in materials where different atomic masses and strong bonds between atoms lead to very high vibrational frequencies [19]. The upturn at the lowest temperature of this measurement motivated our heat-capacity measurements under different fields. C_p/T data for $Ba_4NbIr_3O_{12}$ and $Ba_4NbRh_3O_{12}$ from 1.8 to 10 K under the fields of 0, 1, 5, and 9 T are shown in the inset of Fig. 5. The upturn in the iridate is suppressed by the applied field and there is no upturn seen at an applied field of 9 T. This behavior has recently been observed in materials proposed to be quantum spin liquids [20–24].

Figure 6 shows the heat capacity divided by temperature for both materials measured down to 0.35 K. While $Ba_4NbRh_3O_{12}$ shows a broad anomaly at 1.5 K [Fig. 6(c)] which we suggest is the signature of magnetic ordering, possibly of the spin-glass type, $Ba_4NbIr_3O_{12}$ has a linear upturn in C_p/T below 2 K under $\mu_0 H = 0$ and 1 T applied fields (Fig. 6(a) and Fig. S3 of the Supplemental Material [27]). However, it is suppressed under 2 and 3 T. This behavior was observed in the previously reported spin liquid material $H_3LiIr_2O_6$ [11]. (See Fig. S3 of the Supplemental Material [27] for a log-log plot of our data.) While the extrapolation of heat capacity goes to 0 in the case of $Ba_4NbRh_3O_{12}$ [Fig. 6(d)], the heat capacity extrapolates to 15 mJ/mol-K at 0 K in $Ba_4NbIr_3O_{12}$ (Fig. 6(b) and Fig. S2 of the Supplemental Material [27]). Concerning the nuclear magnetism, a C_p/T vs T plot of IrO_2 from the literature [25] shows the value of about 6.5 mJ/mol$-K^2$ at low temperatures, attributable to nuclear spins. With 3 Ir per formula unit in our Ir material, that would yield about 20 mJ/mol$-K^2$, far below the low-temperature (0.35 K) C_p/T data we report for $Ba_4NbIr_3O_{12}$, which is around 130 mJ/mol$-K^2$. This rules out the possibility of nuclear spin dominating the specific heat in our material and suggests to the authors that $Ba_4NbIr_3O_{12}$ is a spin liquid candidate since the presence of a significant amount of magnetic entropy at low temperatures implies the presence of low-energy spin excitations [20–24]. The heat-capacity data for $Ba_4NbIr_3O_{12}$ below 2 K fits to the function $C_p(T) = kT^\alpha$, where $k = 0.1$ and $\alpha \approx 3/4$, as shown in Fig. 6(b) and Fig. S3 of the Supplemental Material [27]; the power smaller than 1 suggests a possible spin liquid state in this material [11].

The resistivities of $Ba_4NbIr_3O_{12}$ and $Ba_4NbRh_3O_{12}$ are plotted as a function of reciprocal temperature in Fig. S4 of the Supplemental Material [27]. Resistivity data from 200 to 300 K were fit to the standard model $\rho = \rho_o e^{\frac{E_a}{k_b T}}$, and the transport activation energy E_a was calculated to be approximately 0.05 eV for both materials. With the activation energy of 0.05 eV, $Ba_4NbIr_3O_{12}$ and $Ba_4NbRh_3O_{12}$ are both semiconductors, similar to the related trimer-based compounds $Ba_4NbRu_3O_{12}$, $Ba_4LnRu_3O_{12}$, and $Ba_4LnIr_3O_{12}$ [14,26].

IV. CONCLUSION

The materials $Ba_4NbIr_3O_{12}$ and $Ba_4NbRh_3O_{12}$ crystallize in a 12-layer hexagonal perovskite structure in the R-3m space group; Ir_3O_{12} or Rh_3O_{12} trimers are the magnetically active parts of the structure because Ba^{2+} and Nb^{5+} are not magnetic. While $Ba_4NbRh_3O_{12}$ may show some type of magnetic ordering at 1.5 K, the low-temperature heat capacity of $Ba_4NbIr_3O_{12}$ follows a power law between 2 and 0.35 K, implying that the material is a candidate for a spin liquid. First-principles calculations will be of interest to investigate the electronic structure of both materials, in particular to investigate the origin of the relatively low magnetic moments, which appear to the authors to support a "molecular" origin for the magnetism. Pair distribution function (PDF) or high-resolution synchrotron diffraction analysis could be performed to determine whether there is short-range or subtle long-range charge ordering in the trimers. Very low-temperature thermodynamic, heat transport, neutron scattering, and other detailed characterization will be of interest to confirm the presence or absence of a spin liquid state.

ACKNOWLEDGMENTS

This work was supported as part of the Institute for Quantum Matter, an Energy Frontier Research Center funded by the US Department of Energy, Office of Science, Office of Basic Energy Sciences under Award No. DE-SC0019331. The authors thank Tai Kong for discussion on the analysis of the magnetic susceptibilities.

[1] J. Kim, A. H. Said, D. Casa, M. H. Upton, T. Gog, M. Daghofer, G. Jackeli, J. V. D. Brink, G. Khaliullin, and B. J. Kim, Phys. Rev. Lett. **109**, 157402 (2012).
[2] D. Pesin and L. Balents, Nat. Phys. **6**, 376 (2010).
[3] B. J. Kim, H. Jin, S. J. Moon, J.-Y. Kim, B.-G. Park, C. S. Leem, J. Yu, T. W. Noh, C. Kim, S.-J. Oh, J.-H. Park, V. Durairaj, G. Cao, and E. Rotenberg, Phys. Rev. Lett. **101**, 076402 (2008).
[4] G. Jackeli and G. Khaliullin, Phys. Rev. Lett. **102**, 017205 (2009).
[5] B. F. Phelan, J. Krizan, W. Xie, Q. Gibson, and R. J. Cava, Phys. Rev. B **91**, 155117 (2015).
[6] S. Borisenko, D. Evtushinsky, Z. Liu, I. Morozov, R. Kappenberger, S. Wurmehl, B. Büchner, A. Yaresko, T. Kim, M. Hoesch, T. Wolf, and N. Zhigadlo, Physica Status Solidi (b) **254**, 1600550 (2016).
[7] Y. Singh and P. Gegenwart, Phys. Rev. B **82**, 064412 (2010).
[8] S. V. Streltsov, G. Cao, and D. I. Khomskii, Phys. Rev. B **96**, 014434 (2017).
[9] P. Anderson, Mater. Res. Bull. **8**, 153 (1973).
[10] Y. Okamoto, M. Nohara, H. Aruga-Katori, and H. Takagi, Phys. Rev. Lett. **99**, 137207 (2007).
[11] K. Kitagawa, T. Takayama, Y. Matsumoto, A. Kato, R. Takano, Y. Kishimoto, S. Bette, R. Dinnebier, G. Jackeli, and H. Takagi, Nature (London) **554**, 341 (2018).
[12] L. T. Nguyen, T. Halloran, W. Xie, T. Kong, C. L. Broholm, and R. J. Cava, Phys. Rev. Mater. **2**, 054414 (2018).

[13] B. H. Toby, J. Appl. Crystallogr. **34**, 210 (2001).
[14] K. Momma and F. Izumi, J. Appl. Crystallogr. **44**, 1272 (2011).
[15] W. Miiller, M. T. Dunstan, Z. Huang, Z. Mohamed, B. J. Kennedy, M. Avdeev, and C. D. Ling, Inorg. Chem. **52**, 12461 (2013).
[16] Y. Shimoda, Y. Doi, M. Wakeshima, and Y. Hinatsu, J. Solid State Chem. **182**, 2873 (2009).
[17] J. Terzic, J. C. Wang, F. Ye, W. H. Song, S. J. Yuan, S. Aswartham, L. E. Delong, S. V. Streltsov, D. I. Khomskii, and G. Cao, Phys. Rev. B **91**, 235147 (2015).
[18] T. Ferreira, S. M. Heald, M. D. Smith, and H.-C. Z. Loye, Inorg. Chem. **57**, 2973 (2018).
[19] M. Akaogi and E. Ito, Geophys. Res. Lett. **20**, 105 (1993).
[20] J. S. Helton, K. Matan, M. P. Shores, E. A. Nytko, B. M. Bartlett, Y. Yoshida, Y. Takano, A. Suslov, Y. Qiu, J.-H. Chung, D. G. Nocera, and Y. S. Lee, Phys. Rev. Lett. **98**, 107204 (2007).
[21] J. P. Sheckelton, J. R. Neilson, D. G. Soltan, and T. M. Mcqueen, Nat. Mater. **11**, 493 (2012).
[22] S. Yamashita, Y. Nakazawa, M. Oguni, Y. Oshima, H. Nojiri, Y. Shimizu, K. Miyagawa, and K. Kanoda, Nat. Phys. **4**, 459 (2008).
[23] Z. A. Kelly, M. J. Gallagher, and T. M. Mcqueen, Phys. Rev. X **6**, 041007 (2016).
[24] O. Mustonen, S. Vasala, E. Sadrollahi, K. P. Schmidt, C. Baines, H. C. Walker, I. Terasaki, F. J. Litterst, E. Baggio-Saitovitch, and M. Karppinen, Nat. Commun. **9**, 1085 (2018).
[25] B. C. Passenheim and D. C. McCollum, J. Chem. Phys. **51**, 320 (1969).
[26] Y. Shimoda, Y. Doi, M. Wakeshima, and Y. Hinatsu, J. Solid State Chem. **183**, 1962 (2010).
[27] See Supplemental Material at http://link.aps.org/supplemental/10.1103/PhysRevMaterials.3.014412 for trimer-based spin liquid candidate $Ba_4NbIr_3O_{12}$.